Research paper

A study of the parameters affecting the particle velocity in cold-spray: Theoretical results and comparison with experimental data

L. Alonso [*], M.A. Garrido-Maneiro, P. Poza

Durability and Mechanical Integrity of Structural Materials, Rey Juan Carlos University, C/Tulipán s.n., 28933, Spain

ARTICLE INFO

ABSTRACT

Within coating applications, cold-spray is nowadays an extended technique commonly used in environments such as the additive manufacturing or repair industries. The differential factor that leads this approach to be chosen over others is its low deposition temperature. The need for ensuring the resistance and durability of the free-standing components has led to the development of models that can predict the kinetic energy of the particles, which is the main driving parameter affecting the deposit performance. In this study, an optimisation theoretical model, previously developed by the authors, is validated with the experimental exit particle velocity data taken from commercial geometries and using Fluent simulations available in literature. The aim of this work is to relate fundamental parameters in the cold-spray process such as the stagnation conditions, nozzle geometry, powder size or particle velocity. This objective is achieved by creating novel interdependent maps connecting these pivotal data by virtue of the model presented. Several graphs describing the final particle velocity depending on the stagnation pressure and temperature are obtained along with the optimal geometry for a wide range of materials (aluminium, titanium, steel, Inconel 625 and copper). In addition, the analytical model is able to hand over a deposition window of particle sizes and velocities that can be achieved using a specific cold-spray equipment. Both set of maps combined together can be a powerful tool which users and manufacturers can benefit from on the grounds that they do not only provide information about whether a deposition can be achieved or not with a cold-spray equipment but also about the stagnation conditions needed. The results obtained with this methodology reflect the limitations of low and medium-pressure equipment in terms of the maximum particle diameter that can be deposited and constitute a novel advance in the state of art of cold-spray. Moreover, the fundamental parameter regarding the geometry, namely the ratio between the nozzle exit and the nozzle throat diameters, is represented as a function of the above-mentioned parameters.

1. Introduction

Cold-spray has become as a proven technique for preventing and repairing damaged surfaces. New lines of research related to the use of this spraying technique for additive manufacturing (CSAM) are being explored nowadays [1–3]. CSAM can be used to build 3D metal components opening a wide range of possibilities in the manufacturing industry, making it possible to establish a sustainable and environmentally respectful manufacturing process. In this process, feedstock particles are injected into a gas stream at temperatures below their melting point. The gas pressure accelerates the particles to speeds from 300 m/s to 1200 m/s, and the particles then impact onto the substrate surface [4,5]. Consequently, the kinetic energy of the particles is turned into high plastic deformation and heat at the moment of impact. Adhesion between the particles and the substrate is produced by a synergistic effect between metallurgical bonding and mechanical interlocking [6–9]. This energy controls the particle bonding process. Therefore, the

deposits are built from the continuous stacking of sprayed particles. Consequently, the kinetic energy of the particles is revealed as a determinant factor for obtaining reliable components by means of this spraying technique. This energy depends on different parameters. Some of them are related to the spraying conditions, others are correlated to the particles (material properties, shape and size).

Regarding the spraying process, the gas stream is intended to transfer sufficient energy to the particles to ensure their adhesion to the substrate. This gas flow is mainly regulated by the nozzle geometry, the type of gas, temperature, and pressure [4]. Air [10], N_2 [11] and He [12] are commonly used as the propellant gas. Traditionally, He and N_2 are the preferred choices. He, is more appropriate because higher velocities can be attained and transferred to the particles due to its low molecular weight. However, He is exceedingly expensive for extensive use. On the contrary, the particle velocity is reduced when N_2 is chosen,

---

* Corresponding author.
E-mail address: luis.alonso.sanjose@urjc.es (L. Alonso).

due to its higher molecular weight. Nevertheless, this gas is cheaper than He. Therefore, N_2 is the most widely used option in cold-spray applications [13].

Temperature constitutes an energy contribution to the spraying process in the form of heat. The increase in gas temperature improves the gas expansion process through the nozzle, increasing the speed of the particles. Additionally, the higher the gas temperature rises the higher the temperature of the particles, leading to an increased degree of particle softening. This increases the particles' propensity for plastic deformation during the impact process, enhancing the deposition efficiency [14,15]. Several previous studies have reported that the properties of the cold-spray coating may be influenced by the gas pressure [16]. A rise in the pressure of the process gas increases the acceleration of the particles during their transit through the nozzle, allowing to reach significantly higher velocities at the nozzle exit [17]. Therefore, the higher the pressure of the process gas, the higher the kinetic energy of the particles, which enhances the bonding process at the particle–substrate and particle–particle contacts [18].

Additionally, the velocity of the particles at the nozzle exit is governed by their acceleration inside the nozzle, which is determined by the nozzle design. The main geometric parameters defining the nozzle geometry are the divergence ratio, the divergent shape and the divergent section length. Consequently, these geometric parameters are critical to giving particles high velocities at the nozzle exit [19, 20]. Alonso et al. [19] proposed an optimised isentropic analytical model to obtain the optimal profile for the divergent part of the nozzle for the cold-spray process. This model was established considering all dependencies in the integration of the motion equation. The nozzle geometry predicted by this model maximises the drag force on the particle and, consequently, the particle speed. The model was applied onto aluminium powder with an average particle diameter of 10 μm, which was sprayed at a constant pressure of 30 bar at three different spraying temperatures (573 K, 723 K and 873 K). They reported the exit particle velocities for different exit nozzle diameter to nozzle throat diameter ratios, identifying the optimal ratio.

Characteristics of the particles, such as their physical properties, shape and size, have a significant influence on the deposition process. For similar average particle sizes, spherical geometries have lower drag coefficients than irregular ones. Therefore, particles with irregular geometry show a higher velocity than spherical ones. However, a spherical morphology is desired to provide better adhesion strength and denser deposits [21]. Several studies report that smaller particles show higher accelerations due to their lower mass, attaining higher velocities at the nozzle exit [22]. Nevertheless, a physical property that combines size and mass is the density. Therefore, a complementary study concerning the effect of density on the kinetic energy of the particles may be of interest. The effect of density on the characteristics of cold-spray sprayed materials has been studied in combination with other properties such as particle size and specific heat [23]. Previous research has revealed that the density, melting temperature and tensile strength of cold-spray project metals play an important role in determining critical speed [24]. In addition, several models have been proposed for obtaining an estimation of the force and the stress withstood by the particle during the impact. These models depend on particle density; however, they are used to predict deposit characteristics [25]. Furthermore, the gas flow behaviour predicted by the isentropic models through a convergent–divergent transition used to predict particle velocity at the nozzle exit depends on the gas velocity, gas density, gas temperature, gas dynamic viscosity, and drag coefficient; but not on the particle density [19].

Consequently, the authors of this paper observed a lack of analytical studies examining the influence of spraying parameters (pressure, temperature, nozzle geometry, density and geometric characteristics of the particles) on the velocity of the particles at the nozzle exit. Therefore, the purpose of this work was to analyse the effect of these spraying parameters on particle velocity at the nozzle exit due to their

importance for the CSAM industry. Maps of particle velocities were determined by using the analytical model proposed by Alonso et al. [19]. Firstly, this analytical model was validated by comparing experimental measurements reported in bibliography [10,26,27] with simulation predictions of particle velocity at the nozzle exit for the same spraying conditions. Once the model was validated, velocity contour plots were obtained as a function of the stagnation pressure and temperature. In addition, contour plots of the ratio between the nozzle exit and the nozzle throat diameters for two different carrier gases were presented, as a function of the stagnation pressure and temperature: helium (He) and nitrogen (N_2). These maps were obtained for different metallic materials of the sprayed particles in order to observe the influence of density on these velocity contours. Moreover, deposition maps aiming at determining whether adhesion can be achieved depending on the cold-spray equipment available and the powder size were obtained. These results combined together made it possible to identify spraying conditions that optimise the exit velocity of the particles for different densities of the sprayed material, providing a powerful tool for additive manufacturing purposes.

2. Methodology

This section concerns the analytical model previously developed by the authors [19], which is used to obtain the results presented in the next sections of this paper. This model is based on the 1D isentropic gas stream theory by means of a convergent-divergent faucet. In contrast to other models, it considers the dependence of key parameters such as the drag coefficient, the gas density or velocity, as well as pressure and temperature. Under these hypotheses, the problem's governing equation is obtained by means of Newton's second law applied to a sprayed particle on its movement along the divergent region. It can be formulated as

$$\frac{dv_p}{dx} = \frac{C_D \rho A_p}{2 m_p v_p} \left(M \sqrt{\gamma R T} - v_p \right)^2 \tag{1}$$

$$v_p(0) = v_0$$

where v_p is the powder velocity, x, is the longitudinal coordinate of the divergent domain, C_D, is the drag parameter, ρ, is the gas density, A_p, is the particle projected area, m_p, is the particle mass, M, is the Mach number, γ, is a parameter relating the gas heat capacity under isobaric and isochor conditions, R, is the constant of gases and T, is the gas temperature. Integration of Eq. (1) provides the particle velocity along the divergent nozzle region, and, consequently, the exit particle speed when the geometry, and therefore the Mach number, M, is known.

Furthermore, this model can be used to optimise the y-coordinates of the nozzle shape depending on the stagnation conditions. To this end, the function representing the drag force of one particle is maximised considering the particle velocity, v_p, and the Mach number, M, as the two independent variables,

$$F_D = \frac{C_D \rho A_p}{2} \left(M \sqrt{\gamma R T} - v_p \right)^2 \tag{2}$$

where F_D is the drag force associated to a single sprayed-particle. Using the Lagrange multiplier method at each integration step of Eq. (1), the drag force is maximised thanks to the obtaining of the optimal Mach number and thus, the optimal geometry at each integration coordinate is obtained. The system of equations for determining the optimal M at each iteration is the following:

$$\frac{A_p \rho}{2} \left[\frac{dC_D}{dRe_p} \frac{\partial Re_p}{\partial v_p} \left(M \sqrt{\gamma R T} - v_p \right)^2 - 2 C_D \left(M \sqrt{\gamma R T} - v_p \right) \right] = \lambda \tag{3}$$

$$\frac{dC_D}{dRe_p} \frac{\partial Re_p}{\partial M} \rho \left(M \sqrt{\gamma R T} - v_p \right)^2 + C_D \left[\frac{d\rho}{dM} \left(M \sqrt{\gamma R T} - v_p \right)^2 \right.$$

$$\left. + 2\rho \left(M \sqrt{\gamma R T} - v_p \right) \left[\sqrt{\gamma R T} + M \frac{\sqrt{\gamma R T}}{2T} \frac{dT}{dM} \right] \right] = 0 \tag{4}$$
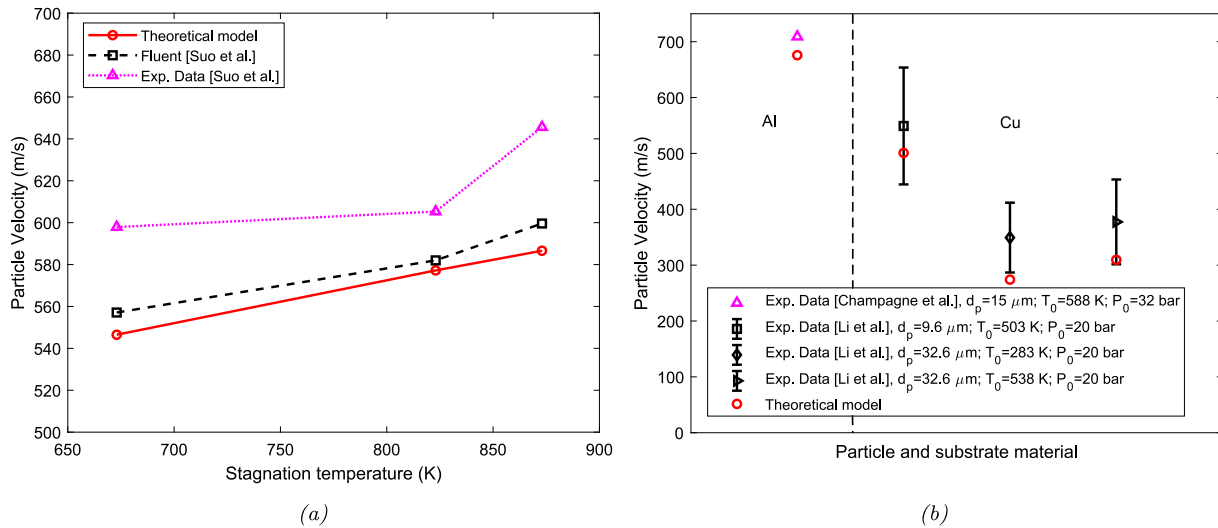
$$v_p = k \tag{5}$$

Fig. 1. (a) Comparison of results of particle velocity vs. stagnation gas temperature obtained experimentally (triangles), with Fluent (squares) and with the theoretical model (circles) for a particle made of ZK61 with a diameter of $d_p = 58$ μm, stagnation pressure of $P_0 = 28$ bar and the nozzle geometry given by Suo et al. [10]. (b) Comparison of results of particle velocity experimentally measured and predicted by the theoretical model for different materials: Al ($d_p = 15$ μm, $T_0 = 588$ K, $P_0 = 32$ bar) [28] and Cu ($d_p = 9.6$ μm, $T_0 = 503$ K, $P_0 = 20$ bar; $d_p = 32.6$ μm, $T_0 = 283$ K, $P_0 = 20$ bar and $d_p = 32.6$ μm, $T_0 = 538$ K, $P_0 = 20$ bar) [29].

where Re_p is the Reynolds number, λ is the Lagrange multiplier and k is the particle velocity (assumed to be constant) at each integration step. The solution of this system of equations coupled with Eq. (6) provides the optimal y-coordinate of the nozzle's divergent region as well as the profile of velocities for all longitudinal coordinates of the nozzle under certain stagnation conditions and with the nozzle diameter at the throat being a known parameter:

$$\frac{A}{A*} = \frac{1}{M}\left[\left(\frac{1}{\gamma+1}\right)\left(1 + \frac{\gamma-1}{2}M^2\right)\right]^{\frac{\gamma+1}{2(\gamma-1)}} \qquad (6)$$

where A is the area perpendicular to the axial coordinate, and $A*$ is this area at the nozzle throat.

3. Validation

The objective of the validation is to evaluate the predictive capability of the model in terms of the final particle speed for a given nozzle shape. To this end, literature has been searched for data regarding exit particle velocity combined with certain geometric parameters. Unfortunately, commercial geometries are generally protected and difficult to obtain. However, the information on geometry reported in some previous works may be enough to validate the model. Geometric details such as the conical geometry of the divergent zone and the diameter proportion given by the throat and the outlet nozzle sections may be sufficient for this purpose. Since it has been demonstrated that the main parameter for determining the final particle speed is the ratio between the throat and the outlet radii, a conical geometry is reconstructed using this parameter to calculate the particle velocity using the model and be able to make a comparison with the data found [19]. First, an experimental validation is carried out and then the validation is extended to numerical results found in the literature.

3.1. Experimental validation

It is highly challenging to find measured data on the particle speed in a cold-spray impact along with nozzle geometry. Suo et al. [10] studied the effect of the stream gas species on particle speed. They were able to measure the exit velocity of a single particle of ZK61 with a diameter of $d_p = 58$ μm subjected to different stagnation temperatures. To that end, they used a laser-based technique, the particle diagnosis system (DPV-2000). Fig. 1(a) represents a comparison between the

particle velocity obtained by Suo et al. [10] (experimental measurements and Fluent predictions) and the particle velocity predicted by the analytical model vs. stagnation temperature. Fig. 1(b) shows additional experimental data that were found for Al [28] and Cu [30] particles. Champagne et al. [28] measured the particle velocity using the DPV-2000 system while [30] benefited from the high velocity oxygen fuel (HVOF) process using an optoelectronic measurement system [31]. Fig. 1(b) compares these data with the particle velocity predicted by the theoretical model for different sizes and stagnation conditions.

Fluent predictions from Suo et al. [10] fit well with the experimental data provided, with differences below 8%. A similar correlation was obtained with the theoretical model. The differences between the Fluent predictions and the results obtained with the theoretical model are practically negligible (below 2%). Furthermore, both models capture the well-known experimental fact that the particle speed and the stagnation temperature are proportional. Moreover, in Fig. 1(b) an excellent agreement is observed for the Al prediction with an error below 5%. As for the Cu results, all the theoretical predictions are within the error bars or slightly below showing an overall decent predictive capability of the model. These narrow variations encourage to use simplified analytical models such as the one proposed in this work instead of more computationally complex and time consuming models. The maneuverability that the theoretical model guarantees in terms of simulating different conditions or geometries while only having to change a few numbers, and the low computational time of each simulation (in the order of seconds), make this model an attractive alternative to be used in the prediction of cold-spray parameters. In addition, it makes it possible to calculate the optimal geometry for any stagnation conditions and particle characteristics.

3.2. Comparison with fluent

Since the model has already been experimentally validated, this section will assess whether it can correctly predict the different trends on particle velocity when different parameters are varied. To prove the consistency of the model, it should be capable of accurately predicting the final particle speed upon the varying of three set of parameters governing the problem: the stagnation conditions, the particle characteristics and the nozzle geometry. Due to the lack of a wide range of experimental data available, Fluent simulations are used to assess the trends that the analytical model should predict. The above-mentioned comparisons can be performed according to the three sets.
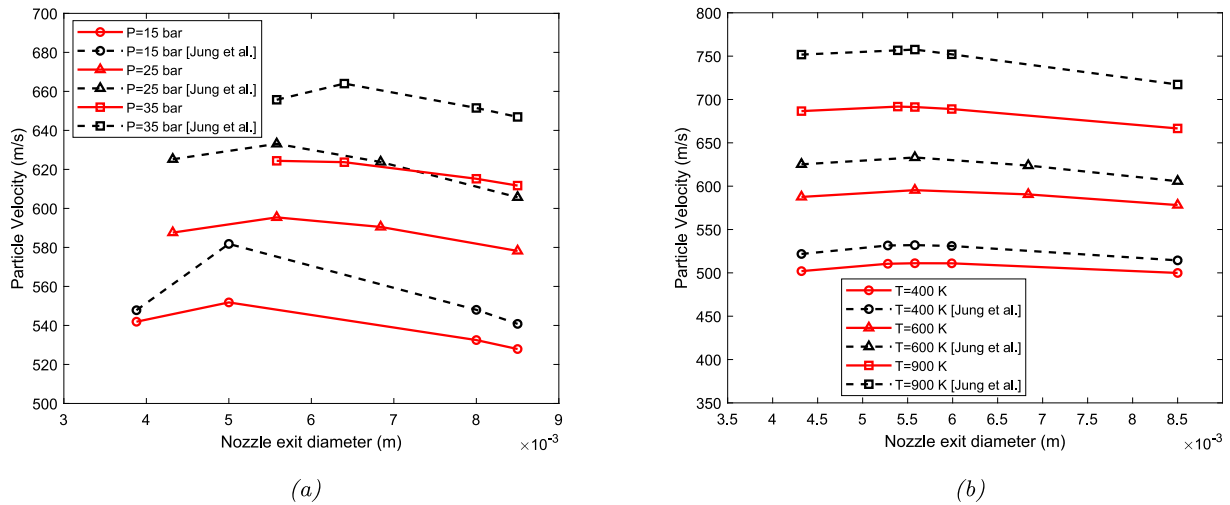
(a)

(b)

Fig. 2. Comparison between the Fluent data and the theoretical model of particle velocity vs. final nozzle diameter: Effect of (a) gas pressure for a fixed stagnation temperature of $T_0 = 600$ K, (b) gas temperature for a fixed stagnation temperature of $P_0 = 25$ bar on optimal nozzle exit diameter, for a particle made of Al with a diameter of $d_p = 15$ μm and the nozzle geometry given by Jung et al. [32].

Regarding the stagnation conditions, Jung et al. [32] addressed how pressure and temperature control the particle velocity. Fig. 2 shows similarity when the theoretical model results are compared with the ones predicted by Jung et al. [32]. Figs. 2(a) and 2(b) show the particle velocity (Al, $d_p = 15$ μm) vs. the nozzle exit diameter as a function of different pressures and temperatures, respectively.

Good agreement is observed between the two models. The particle velocity increases with pressure and temperature as expected in both models. In terms of the predicted trends, both models present a convex curvature with a maximum in between the extreme values of the exit diameter. From Fig. 2(a) it can be inferred that, as the pressure increases, the maximum is reached with larger nozzle exit diameters. Nevertheless, the optimal nozzle exit diameter appears to be constant with temperature (Fig. 2(b)). Note that all the curves are reasonably flat, especially in Fig. 2(b), even though the diameter is doubled. This means that the particle speed is not very susceptible to the expansion ratio for this particle material and diameter. This is in accordance with the results given by the optimisation model developed by Alonso et al. [19]. In that study, an optimal region for particle velocity was predicted. This region was depicted as a proportion between the nozzle exit and nozzle throat diameters. Alonso et al. [19] reported a rather flat evolution of this diameter ratio that ranged between 2 and 4. The ratio shown in Fig. 6 is included approximately between 2 and 3. Consequently, the results of the analytical model agree with to those addressed by Alonso et al. [19].

The impact of the particle's dimensions on its velocity is an essential feature to be captured by the model if different powder feed-stocks with different sizes are used. In this regard, Li et al. [26] conducted simulations within an ample spectrum of particle sizes (from $d_p = 5$ μm to $d_p = 50$ μm). Fig. 3 presents the predictions of the theoretical approach as well as Li et al. [26]'s results for particle speed vs. nozzle exit diameter for different particle diameters, and for stagnation pressure and temperature of $P_0 = 25$ bar and $T_0 = 573$ K. The conical geometry used is described in full in [26].

According to Fig. 3, smaller and, consequently (provided they have the same density), lighter particles are propelled to higher velocities under the same conditions. This is backed up by the energy and momentum conservation laws, so the model is physically consistent. Moreover, the predicted trends are the same with both models, with the difference being a more or less constant offset. Again, as explained above, the correlation between particle speed and nozzle exit dimension is not strong within the ranges analysed.

Nozzle geometry is the last check to prove the theoretical model can be adapted to any condition. Li et al. [26] analysed the influence of two
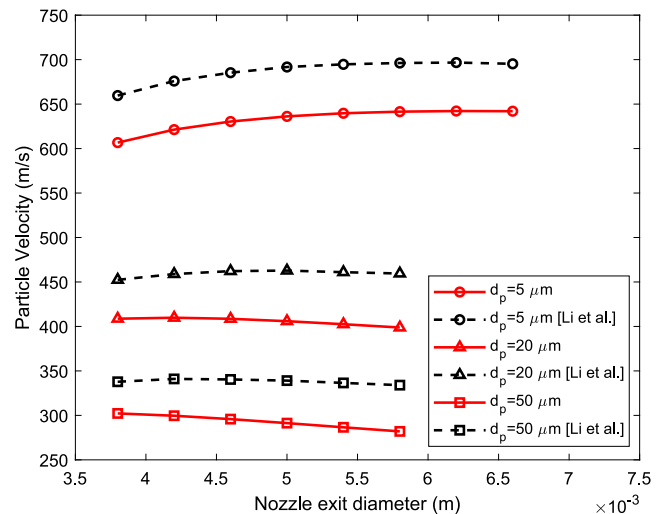

Fig. 3. Comparison between the Fluent data and the theoretical model of particle velocity vs. nozzle exit diameter: Variation of the optimal nozzle exit diameter as a consequence of particle diameter, for stagnation pressure and temperature of $P_0 = 25$ bar and $T_0 = 573$ K, for a particle made of 316L stainless steel and the nozzle geometry given by Li et al. [26].

of the overriding dimensions regarding nozzle geometry: the divergent length and the nozzle throat diameter. Figs. 4(a) and 4(b) represent the predictions of the theoretical model as well as Li et al. [26]'s results for particle velocity vs. nozzle exit diameter for different divergent lengths and nozzle throat diameters, for stagnation pressure and temperature of $P_0 = 25$ bar and $T_0 = 573$ K, respectively. The conical geometry used is described in full in Li et al. [26].

Fig. 4 reveals that larger divergent lengths point to higher particle speeds as expected. The trend of both models is almost identical for the $L_d = 0.12$ m case with a difference below 7%. Better matching results are obtained for the $L_d = 0.27$ m case in terms of the differences observed. However, the curves seem to diverge from the starting point. Both models are consistent with the flat behaviour as the nozzle exit diameter varies. Moreover, the results with different nozzle throat diameters, while keeping the expansion ratios constant, are compared in Fig. 4(b). Even though the trends are dissimilar, both models show a very slight variation in particle velocity when the expansion ratio is kept constant.
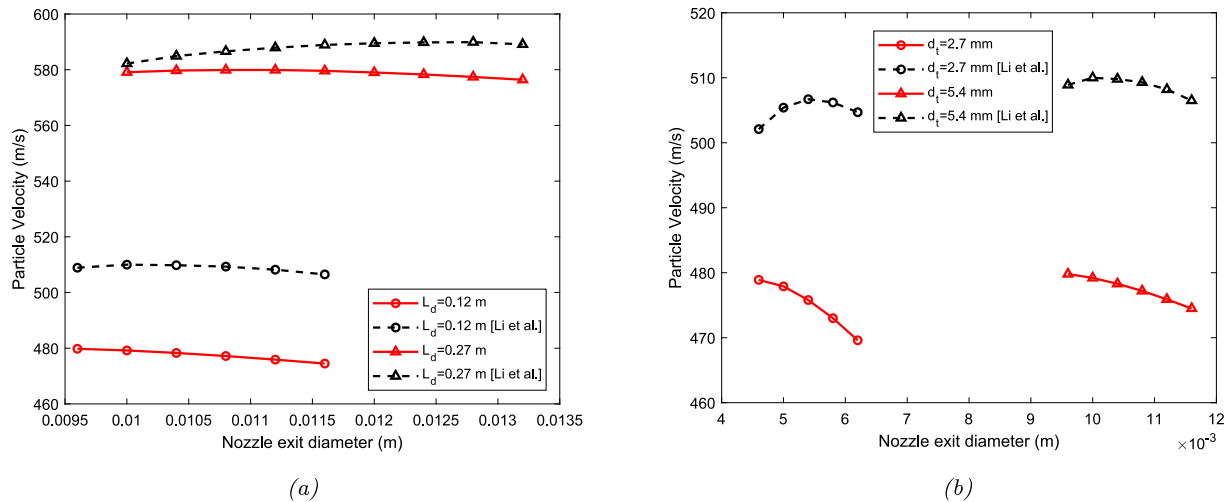
(a)

(b)

Fig. 4. Comparison between the Fluent data and the theoretical model of particle velocity vs. nozzle exit diameter: Effect of (a) divergent length with a throat diameter of $d_t = 0.0027$ m, (b) throat diameter with a divergent length of $L_d = 0.12$ m on optimal nozzle exit diameter, for stagnation pressure and temperature of $P_0 = 25$ bar and $T_0 = 573$ K, for a particle made of 316L stainless steel with a diameter of $d_p = 20$ μm and the nozzle geometry given by Li et al. [26].
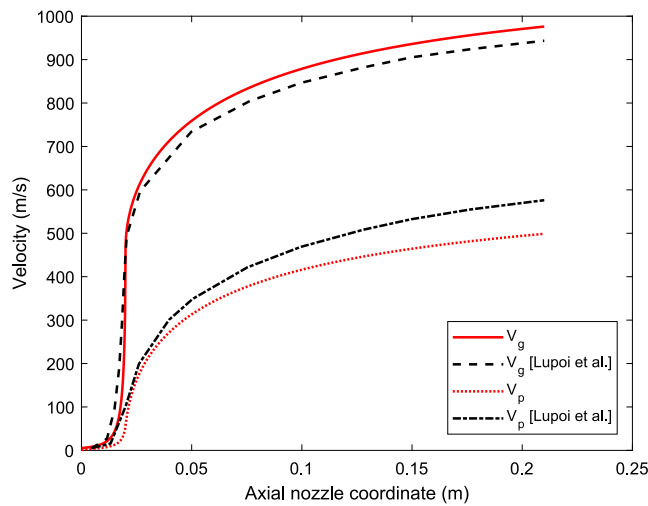

Fig. 5. Representation of the Fluent and theoretical results of particle and gas velocities (nitrogen) vs. the longitudinal nozzle coordinate for stagnation pressure and temperature of $P_0 = 30$ bar and $T_0 = 623$ K, for a particle made of Ti with a diameter of $d_p = 45$ μm and the nozzle geometry given by Lupoi [27].

Up to this point, the results provided by the theoretical model show a good degree of agreement with the experiments and simulations found in literature. However, these results only account for magnitudes at the end of the nozzle without knowing if what happens inside the nozzle is predictable. Although it is impossible to monitor the velocity of a single particle experimentally during its path through the nozzle, it can be compared with other simulations in literature. To this end, a comparison between theoretical and Fluent simulations found in literature [27] for gas and particle velocities (Ti, $d_p = 45$ μm) is shown in Fig. 5. A conical geometry was used to carry out these simulations, with an input diameter of $d_i = 20$ mm, a throat diameter of $d_p = 2.7$ mm, an exit diameter of $d_p = 7.8$ μm, a convergent length of $L_c = 20$ mm and a divergent length of $L_c = 190$ mm.

According to Fig. 5, the gas velocity curves are practically identical in qualitative terms, and present small quantitative differences. Both models predict a steep change at the beginning of the nozzle followed by a smoother curve. They differ to a greater degree with regard to particle velocity (always below the 14%), although the trend is similar. It can be inferred from this that the transfers of energy and momentum

between the particles is lower in the theoretical model due to the different methods of resolution. Nevertheless, both are believed to be valid approximations of actual particle velocities.

Overall, it has been shown that the theoretical model can reasonably predict experimental measurements of particle velocity in the cold-spray process as displayed in Fig. 1(a), and is a powerful tool in terms of simplicity, maneuvrability and computational time. In addition, the comparison with Fluent simulations from literature reveals that theoretical predictions of particle velocity are quite similar to Fluent predictions. Moreover, the trends predicted by both models are in agreement when crucial parameters such as the stagnation conditions, particle characteristics or nozzle geometry are varied.

4. Results

In this section, the above-mentioned theoretical model was used to obtain the results presented. Note that all the results presented below refer to the optimal geometry provided by the analytical formulation and are obtained for a particle diameter of $d_p = 10$ μm. An analysis of the control that the powder metal exercises is performed in terms of the final particle speed, depending on the stagnation parameters. The results are divided into low-density powder metals such as aluminium and titanium and high-density powder metals such as steel, Inconel 625 and copper. Different maps of the final particle speed are shown, depending on the stagnation parameters for several densities. Moreover, information about the optimal geometry for obtaining the final particle velocity is provided by means of the relationship between the exit and the nozzle throat diameters, with the latter and the divergent region dimension being fixed ($D_{nt} = 0.0015$ m and $L_f = 0.1$ m). In addition, the relevance of the two most common carrier gases in the process (nitrogen and helium) is measured qualitatively and quantitatively for all the powder metals studied. Finally, a methodology to obtain a deposition window for any material and particle size hinging on the features of any specific cold-spray equipment is implemented.

4.1. Analysis of low density powder metals

The main purpose of this analysis is to provide exit particle velocity maps for aluminium and titanium for different stagnation conditions, and impose the optimal nozzle y-coordinates defined by the analytical model described in Section 2. Furthermore, the most important geometric features regarding the maximisation of the final particle speed are the nozzle exit and nozzle throat diameters [19]. That is the
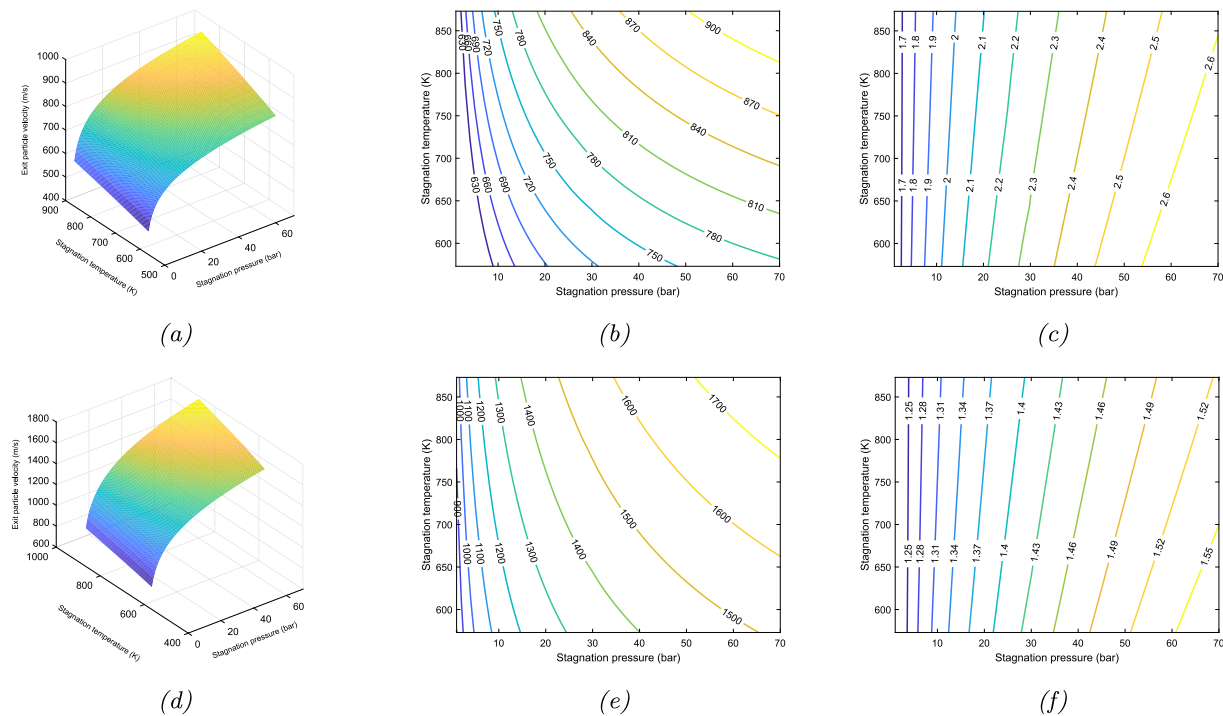
Fig. 6. (a), (d) Exit particle velocity, (b), (e) contour plots, and (c), (f) proportion between the nozzle exit and nozzle throat diameters, in terms of the stagnation pressure and temperature, for Aluminium as the powder metal. (a), (b), (c) Nitrogen and (d), (e), (f) Helium as the stream gas.

reason why these maps are also presented. Figs. 6(a) and 6(d) show the resulting surfaces of the final particle velocity for a bounded range of stagnation pressures and temperatures for aluminium, as the powder metal, and nitrogen and helium, as the carrier gases, respectively. For a better understanding of Figs. 6(a) and 6(d), Figs. 6(b) and 6(e) show the contour plots of constant final particle velocities. In addition, the proportion between the nozzle exit and nozzle throat diameters is shown in Figs. 6(c) and 6(f). This ratio is of special interest because it can be used to build a conical geometry reasonably close to the optimal one provided by the analytical model if the outcomes of the exit particle velocity are compared.

Fig. 6(b) confirms that the correlation between the stagnation parameters, namely pressure and temperature, is inversely proportional for a constant exit particle velocity. This relationship becomes more evident as exit particle velocity increases. A comparison of Figs. 6(b) and 6(e) proves that the exit particle speed is remarkably higher if helium is used as the stream gas for the same stagnation status. Furthermore, the final particle speed increases at a slower pace if the stagnation pressure is increased regardless of the choice of gas. However, the same behaviour is not observed when raising the stagnation temperature; in this case, the exit particle speed instead increases constantly for both of them. For a better understanding of Figs. 6(c) and 6(f), a parameter measuring conicity needs to be defined. Fig. 7 shows a scheme of the optimal geometry provided by the analytical model, together with a conical geometry (built using the diameters given by the analytical model in Figs. 6(c) and 6(f)). Although all the results presented were obtained using the analytical model, the conical alternative yields reliable results that are very close to the optimal geometry, and is mainly used in the manufacturing industry. That is why figures depending on the ratio of diameters will be analysed in terms of conicity.

In view of Fig. 7 the angle of conicity is defined as follows:

$$\alpha = tan^{-1}\left(\frac{D_e - D_{nt}}{2L_f}\right) \tag{7}$$

where L_f is the length of the divergent part of the nozzle and D_e and D_{nt} are the nozzle exit and nozzle throat diameters, respectively. Figs. 6(c) and 6(f) show how the final particle speed increases with the

angle of conicity. Therefore, Fig. 6(c) compared to Fig. 6(f) reflects that the required angle of conicity is clearly smaller if helium is used as the stream gas. In fact, the maximum angle of conicity needed to obtain a velocity around 1700 m/s with helium is approximately $\alpha = 0.24°$ while the one required to reach a velocity nearly 630 m/s with nitrogen is $\alpha = 0.3°$, showing that a smaller angle is needed to obtain a remarkably higher velocity when using He as the carrier gas.

Figs. 8(a)–8(c) represent the exit particle velocity in relation to stagnation conditions, the velocity contour plots for stagnation temperature vs. stagnation pressure and the contour plots of the proportion between the nozzle exit and nozzle throat diameters for stagnation temperature vs. stagnation pressure, respectively, for titanium, using nitrogen as the stream gas. Figs. 8(d)–8(f) are the same but with helium replacing nitrogen as the carrier gas.

Regarding the trends related to the comparison between nitrogen and helium, Fig. 8 shows the same behaviour as Fig. 6. Therefore, the qualitative improvement when using helium and the reduction of the angle of conicity are independent of the density of the powder metal. Additionally, the shapes of the curves in Figs. 6 and 8 are the same. Moreover, a slightly higher exit particle velocity is obtained for aluminium when stagnation pressure and temperature are kept constant, due to its lower density. In addition, Figs. 8(c) and 8(f) show lower conicity compared to Figs. 6(c) and 6(f), as demonstrated by Alonso et al. [19].

4.2. Analysis of high density powder metals

To compare the trends of the maps obtained for the low-density powder metals, a complete study using three of the most common high-density powder metals was performed. To this end, steel, Inconel 625 and copper, which are important in various repairing applications, were chosen to carry out the study. Figs. 9(a) and 9(d) show the exit particle velocity for a wide range of stagnation pressures and temperatures, with steel as the powder metal and nitrogen and helium as the carrier gases, respectively, and the corresponding contour plots are also represented in Figs. 9(b) and 9(e). Figs. 9(c) and 9(f) describe
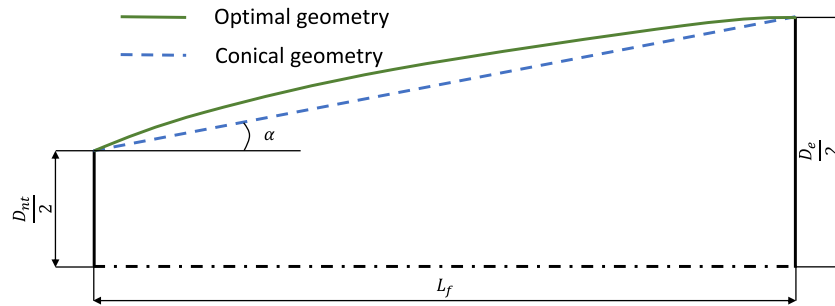
Fig. 7. Schematic representation of the optimal (straight line) and conical (dashed line) geometries for the divergent part of the nozzle.
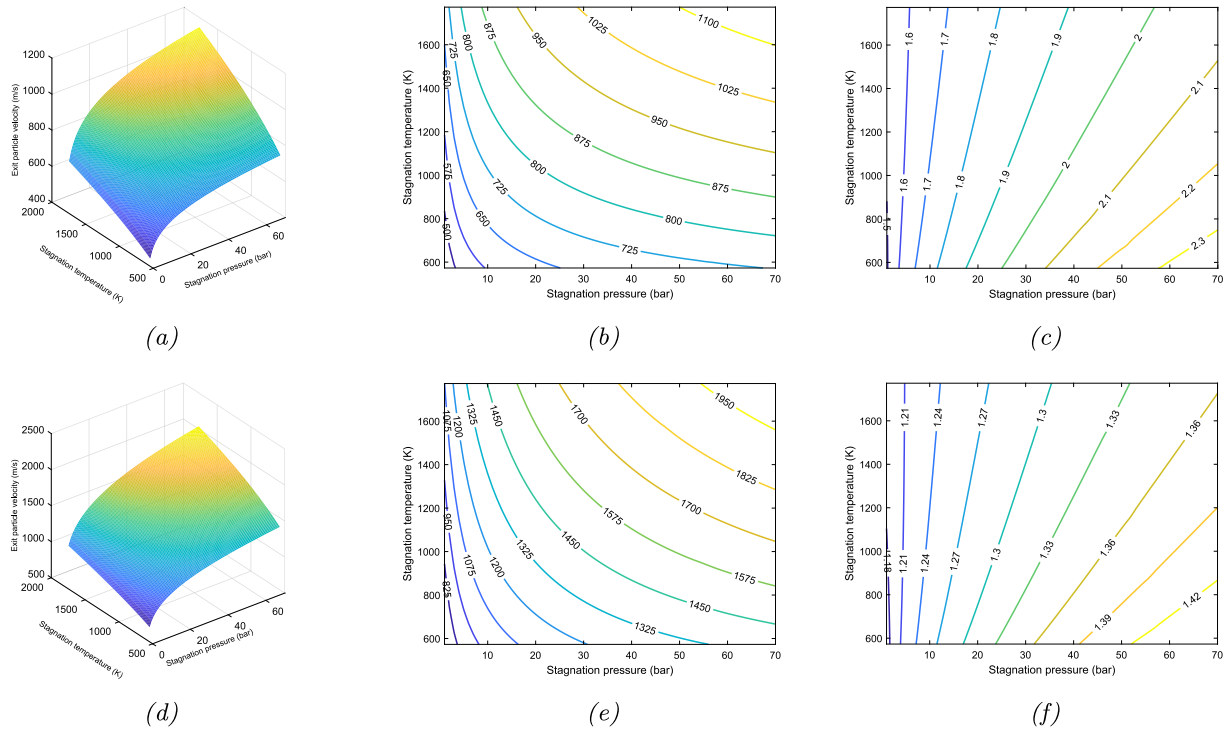

Fig. 8. (a), (d) Exit particle velocity, (b), (e) contour plots, and (c), (f) proportion between the nozzle exit and nozzle throat diameters, in terms of the stagnation pressure and temperature, for Titanium as the powder metal and (a), (b), (c) Nitrogen and (d), (e), (f) Helium as the stream gas.

the ratio of diameters as a function of the same parameters for both carrier gases.

The steel particles (Fig. 9) qualitatively exhibit the same behaviour as the aluminium and titanium particles shown in Figs. 6 and 8. Comparing the results depicted in Figs. 6 and Fig. 8 with those shown in Fig. 9, the exit velocity is higher for low-density powder metals as a result of their lower density and, thus, the greater ease with which they are carried along the nozzle.

Figs. 10(a) and 11(a), and 10(d) and 11(d) show the exit particle velocity with varying stagnation conditions for Inconel 625 and copper as the powder metal and nitrogen and helium as the carrier gases, respectively, and Figs. 10(b) and 11(b), and 10(e) and 11(e) show the corresponding contour plots. Figs. 10(c) and 11(c), and 10(f) and 11(f) illustrate the ratio of diameters as a function of the same parameters for both metal powders and both carrier gases.

In view of Figs. 10 and 11, the results show that the model's predictions are consistent when the density of the particles increases. In this regard, the final particle speed, as well as conicity, decreases as the density of the particle increases. Although the behaviour of these trends may not be so evident for high-density powder metals, due to the small differences in density, all the cases analysed follow the same pattern with regard to the final particle speed and conicity. This can

be seen more clearly if particle metals separated according to a low-high density threshold are examined. Overall, different maps of the final particle speed, as well as the ratio of diameters of the nozzle's divergent domain, as a function of the stagnation parameters, obtained with the optimisation analytical model, are presented for a wide range of particle materials/densities for the most common carrier gases used.

4.3. Deposition windows

When analysing deposition conditions, it is a well-established fact that the impact velocity of the particle must be within certain low and a high boundaries describing the non-adhesion and erosion limits, respectively, to achieve adhesion [5]. The need for discerning if a cold-spray equipment has the capacity to provide the necessary conditions to accomplish bonding for a certain material and particle size seems a compelling reason to elaborate a theoretical guide to elucidate it. In Fig. 12 the dot-dash green, dash red and solid black lines represent the maximum obtainable particle velocity vs. the particle diameter predicted by the analytical model for typical low-pressure (T_{0max} = 873 K, P_{0max} = 6 bar), medium-pressure (T_{0max} = 873 K, P_{0max} = 30 bar) and high-pressure (T_{0max} = 1273 K, P_{0max} = 60 bar) cold-spray equipment, respectively, for Ti 12(a) and Cu 12(b).
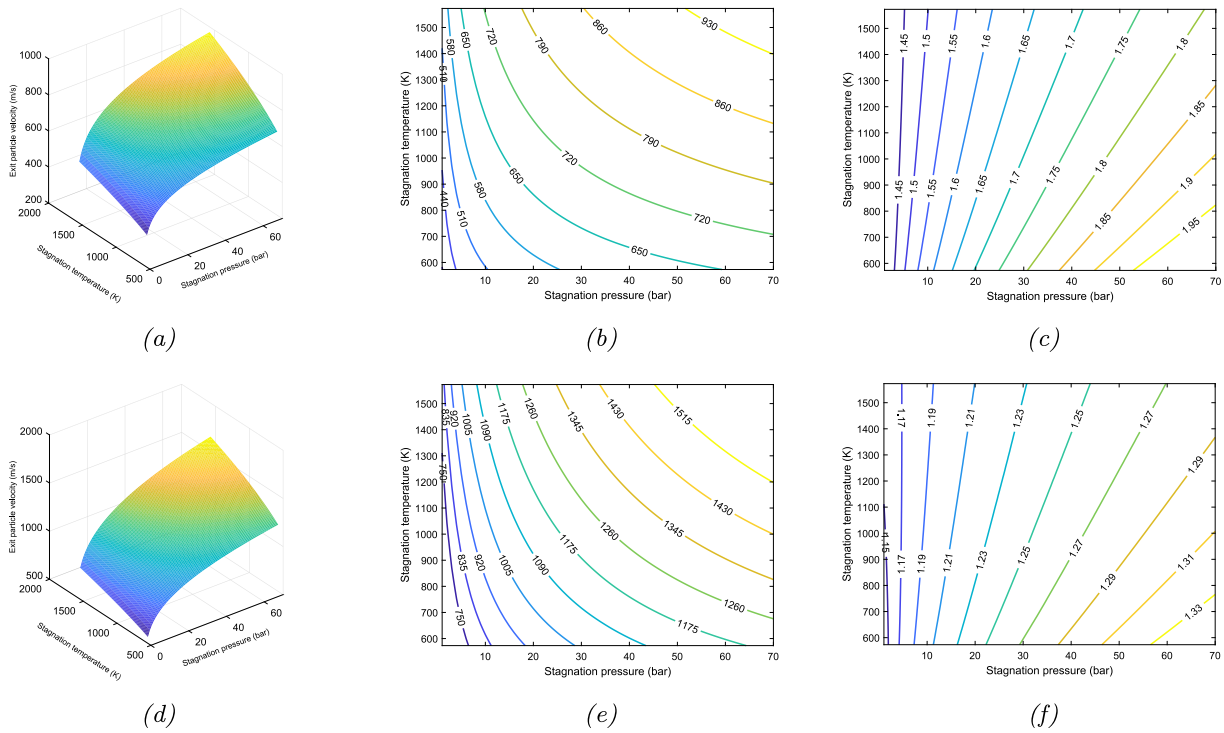
Fig. 9. (a), (d) Exit particle velocity, (b), (e) contour plots, and (c), (f) proportion between the nozzle exit and nozzle throat diameters, in terms of the stagnation pressure and temperature, for Steel as the powder metal and (a), (b), (c) Nitrogen and (d), (e), (f) Helium as the stream gas.
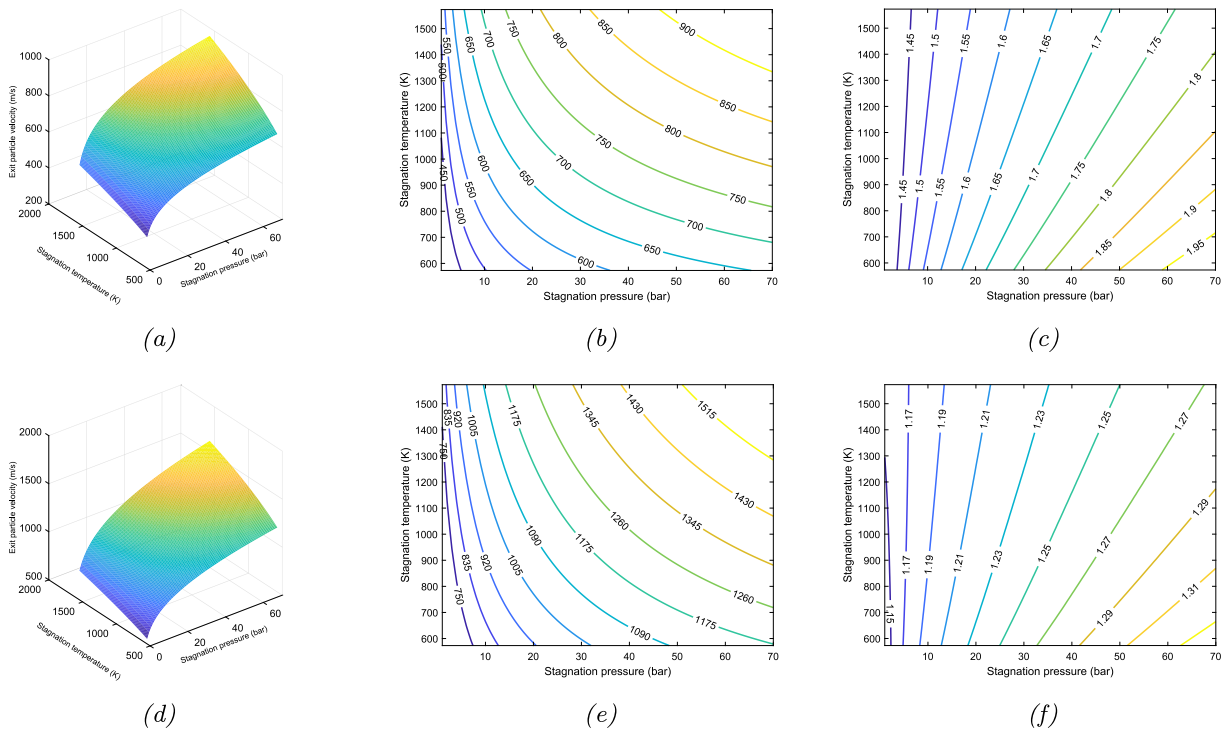

Fig. 10. (a), (d) Exit particle velocity, (b), (e) contour plots, and (c), (f) proportion between the nozzle exit and nozzle throat diameters, in terms of the stagnation pressure and temperature, for Inconel 625 as the powder metal and (a), (b), (c) Nitrogen and (d), (e), (f) Helium as the stream gas.

The intersection between the non-adhesion and erosion limits and the maximum particle velocity curve encloses an area characterising all the possible particle velocity-particle diameter pairs compatible with the cold-spray equipment used. For instance, if the particle diameter is fixed to $d_p = 15$ μm in Fig. 12(a) and the desired velocity is defined by

point B, a medium-pressure cold-spray equipment is able to accelerate the particle up to the desired velocity because point B is inside the red + grey region. On the contrary, if the desired velocity is designated by point A, it cannot be achieved using the same equipment. Additionally, Figs. 12(a) and 12(b) give insight into the maximum particle diameter
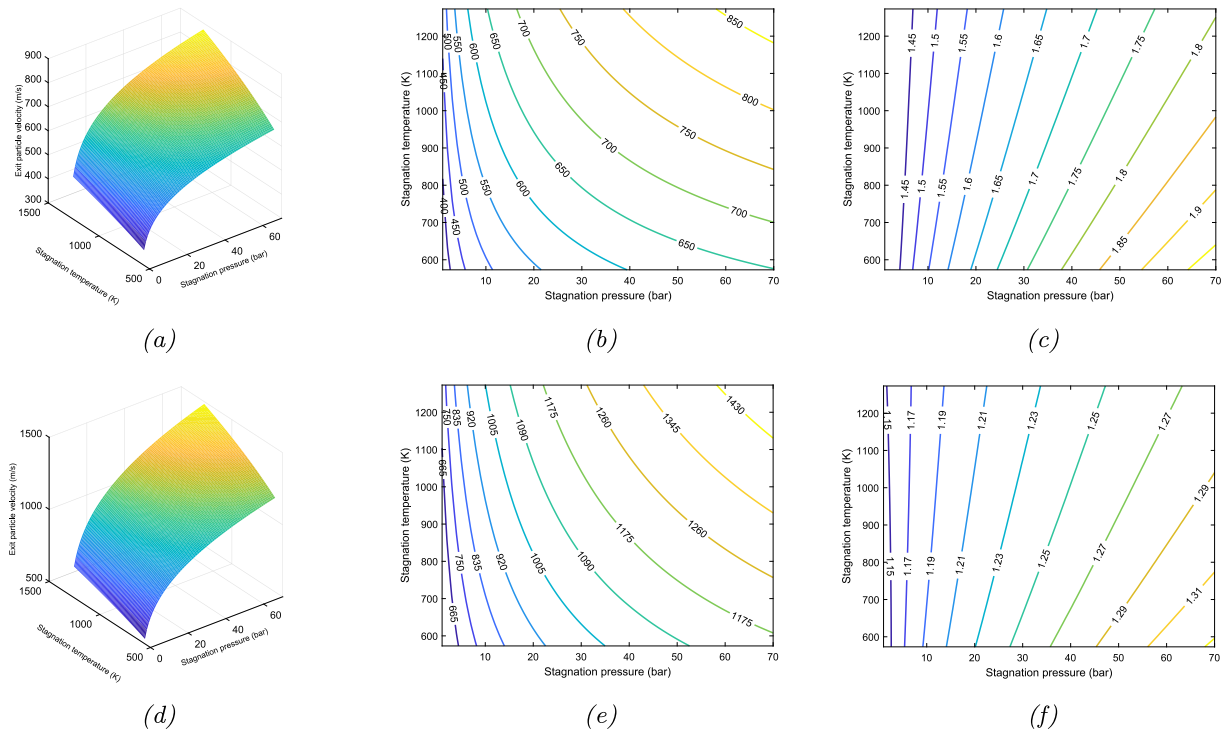
Fig. 11. (a), (d) Exit particle velocity, (b), (e) contour plots, and (c), (f) proportion between the nozzle exit and nozzle throat diameters, in terms of the stagnation pressure and temperature, for Copper as the powder metal and (a), (b), (c) Nitrogen and (d), (e), (f) Helium as the stream gas.
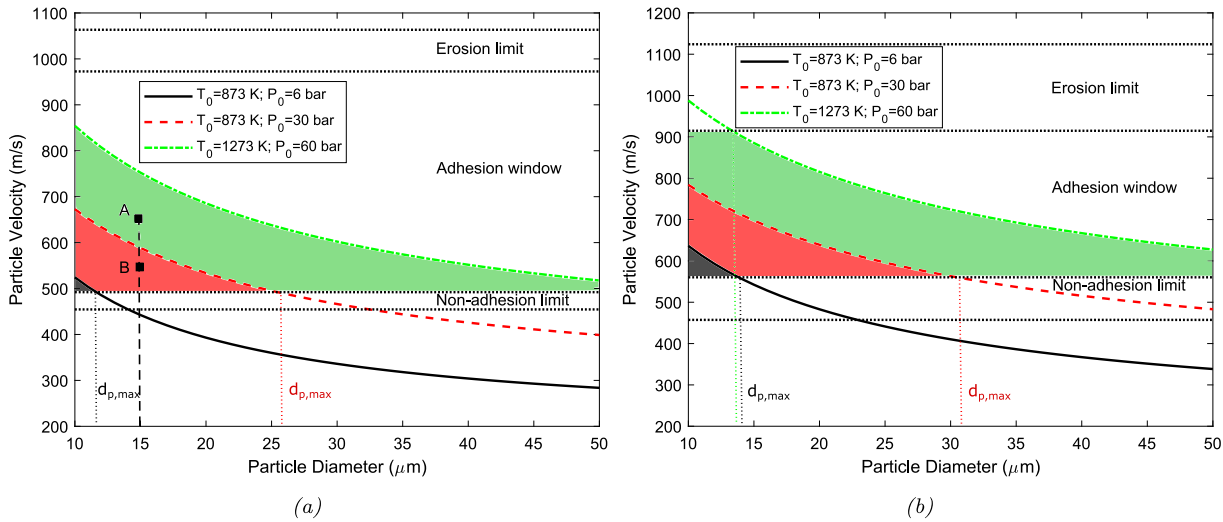

Fig. 12. Maximum obtainable particle velocity vs. particle diameter predicted by the analytical model for low-pressure (solid black), medium-pressure (dash red) and high-pressure (dot-dash green) cold-spray equipment. Coloured areas represent the admissible diameters that can be successfully deposited for a low-pressure (grey), medium-pressure (grey + red) and high-pressure (grey + red + green) cold-spray equipment and their corresponding velocities for (a) Ti and (b) Cu. Non-adhesion and erosion limits are approximate values extracted from Schmidt et al. [33]. (For interpretation of the references to colour in this figure legend, the reader is referred to the web version of this article.)

that can be successfully deposited when using Ti or Cu respectively, $d_{p,max}$, for a specific cold-spray device. On the grounds that these maps can be theoretically reproduced for any nozzle geometry, material and cold-spray equipment, it is imperative to appraise their effectiveness. This goal can be achieved by representing an experimental point in these maps. The work performed by Champagne et al. [28] has been chosen to be represented in Fig. 13 because of the availability of the data needed.

Fig. 13 illustrates that the experimental point obtained by Champagne et al. [28] is inside the compatible region of particle velocity-particle diameter pairs according to the cold-spray equipment described by Champagne et al. [28]. Overall the graphs shown in this subsection

help answering fundamental questions such as if a particle can be accelerated to a specific velocity with a cold-spray equipment or the maximum particle diameter that can be used to achieve adhesion. In fact, as soon as these questions are answered, plots from Sections 4.1 and 4.2 are recalled to yield the necessary stagnations conditions to reach a certain velocity, connecting the entire process.

5. Conclusions

A previously developed analytical model based on the one-dimensional isentropic gas theory, which is able to predict aspects
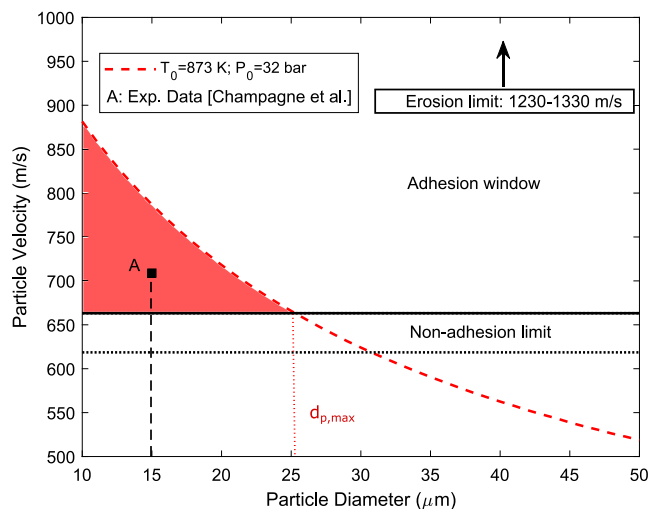
Fig. 13. Maximum obtainable particle velocity vs. particle diameter predicted by the analytical model for a medium-pressure cold-spray equipment [28]. The red area represents the admissible diameters that can be successfully deposited and their corresponding velocities for Al. Point A accounts for the experiment performed by Champagne et al. [28], which is inside the admissible (red) area. Non-adhesion and erosion limits are approximate values extracted from Schmidt et al. [33]. (For interpretation of the references to colour in this figure legend, the reader is referred to the web version of this article.)

such as final particle speed or optimal nozzle geometry, was experimentally validated in this study. To do so, a few examples found in literature providing the final particle speed along with the geometric characteristics of the nozzle were used. With these inputs, a comparison with experimental data for ZK61, aluminium and copper was possible. Within the cases analysed, good correlation was found, with maximum differences lower than 10%. Therefore, the model was proved to successfully simulate exit particle velocity, reproducing the conditions of real experiments. Moreover, the trends when varying different governing parameters, such as the stagnation conditions, particle characteristics or nozzle geometry, were found to be in agreement with Fluent simulations found in literature.

Once the model was validated against experimental results, a set of maps is obtained, describing the exit particle velocity in terms of the stagnation pressure and temperature. Different powder particles within a wide range of densities were studied, from aluminium ($\rho = 2800$ kg/m^3) to copper ($\rho = 8960$ kg/m^3). Furthermore, the two most common gases, helium and nitrogen, were chosen as the stream gas in the simulations. In addition, the ratio between the exit and throat particle diameters was shown for the powder metals and gases mentioned above. A remarkable improvement was observed when helium was used as the carrier gas. In fact, with some metals such as aluminium, the particle velocity almost doubled when using helium in agreement with experimental findings. The required conicity also diminishes when using helium. Another interesting result revealed by this study is that the particle velocity increases to a lesser extent as stagnation pressure rises. However, exit particle velocity increases constantly as stagnation temperature rises. Furthermore, an inversely proportional relationship between stagnation pressure and temperature, while keeping exit particle velocity constant, was observed for all the densities studied. Moreover, in the density range studied, exit particle velocity decreased for higher densities as it is more energy-expensive to carry a heavier particle. With regard to the geometry's dependence on particle density, it was shown that the relationship between the ratio of the nozzle exit and nozzle throat diameters and density is inversely proportional, regardless of the carrier gas used.

Apart from the qualitative trends observed, a set of maps was obtained to quantify the adhesion window of a specific cold-spray

equipment in terms of particle velocity-particle diameter pairs. These graphs allow to predict if adhesion occurs or to determine the maximum powder diameter to deposit a particle. If combined with the plots described above, they can include or discard particle velocity-particle diameter pairs and predict the stagnation conditions required to achieve a certain velocity once deposition is guaranteed. This information constitutes a quantitative guide for users and manufacturers that could be especially relevant for selecting the optimal cold-spray conditions to manufacture a component using the CSAM technique.

CRediT authorship contribution statement

L. Alonso: Writing – review & editing, Writing – original draft, Visualization, Validation, Supervision, Software, Methodology, Investigation, Formal analysis, Data curation, Conceptualization. **M.A. Garrido-Maneiro:** Writing – review & editing, Writing – original draft, Supervision, Project administration, Methodology, Funding acquisition, Conceptualization. **P. Poza:** Writing – review & editing, Supervision, Resources, Project administration, Methodology, Funding acquisition, Conceptualization.

Declaration of competing interest

The authors declare that they have no known competing financial interests or personal relationships that could have appeared to influence the work reported in this paper.

Data availability

Data will be made available on request.

References

[1] X. Wang, F. Feng, M.A. Klecka, M.D. Mordasky, J.K. Garofano, T. El-Wardany, A. Nardi, V.K. Champagne, Characterization and modeling of the bonding process in cold spray additive manufacturing, Addit. Manuf. 8 (2015) 149–162, http://dx.doi.org/10.1016/j.addma.2015.03.006.

[2] S. Yin, P. Cavaliere, B. Aldwell, R. Jenkins, H. Liao, W. Li, R. Lupoi, Cold spray additive manufacturing and repair: Fundamentals and applications, Addit. Manuf. 21 (2018) 628–650, http://dx.doi.org/10.1016/j.addma.2018.04.017.

[3] H. Wu, X. Xie, M. Liu, C. Verdy, Y. Zhang, H. Liao, S. Deng, Stable layer-building strategy to enhance cold-spray-based additive manufacturing, Addit. Manuf. 35 (2020) 101356, http://dx.doi.org/10.1016/j.addma.2020.101356.

[4] A. Papyrin, V. Kosarev, S. Klinkov, A. Alkhimov, V. Fomin, Cold Spray Technology, Elsevier, 2006, http://dx.doi.org/10.1016/B978-0-08-045155-8.X5000-5.

[5] P. Poza, M.Á. Garrido-Maneiro, Cold-sprayed coatings: Microstructure, mechanical properties, and wear behaviour, Prog. Mater. Sci. 123 (2022) http://dx.doi.org/10.1016/j.pmatsci.2021.100839.

[6] H. Assadi, F. Gärtner, T. Stoltenhoff, H. Kreye, Bonding mechanism in cold gas spraying, Acta Mater. 51 (15) (2003) 4379–4394, http://dx.doi.org/10.1016/S1359-6454(03)00274-X.

[7] M. Grujicic, C. Zhao, C. Tong, W. Derosset, D. Helfritch, Analysis of the impact velocity of powder particles in the cold-gas dynamic-spray process, Mater. Sci. Eng. A 368 (1–2) (2004) 222–230, http://dx.doi.org/10.1016/j.msea.2003.10.312.

[8] M. Hassani-Gangaraj, D. Veysset, V.K. Champagne, K.A. Nelson, C.A. Schuh, Adiabatic shear instability is not necessary for adhesion in cold spray, Acta Mater. 158 (2018) 430–439, http://dx.doi.org/10.1016/j.actamat.2018.07.065.

[9] A.S. Perna, A. Viscusi, R.D. Gatta, A. Astarita, Cold spraying on polymer-based composites: Understanding the single-particle adhesion, Surf. Coat. Technol. 447 (2022) 128837, http://dx.doi.org/10.1016/j.surfcoat.2022.128837, URL https://www.sciencedirect.com/science/article/pii/S0257897222007587.

[10] X. Suo, S. Yin, M.-P. Planche, T. Liu, H. Liao, Strong effect of carrier gas species on particle velocity during cold spray processes, Surf. Coat. Technol. 268 (2015) 90–93, http://dx.doi.org/10.1016/j.surfcoat.2014.04.039.

[11] P. Sirvent, M. Garrido-Maneiro, C. Munez, P. Poza, S. Vezzu, Effect of higher deposition temperatures on the microstructure and mechanical properties of Al 2024 cold sprayed coatings, Surf. Coat. Technol. 337 (2018) 461–470, http://dx.doi.org/10.1016/j.surfcoat.2018.01.055.

[12] T. Liu, J.D. Leazer, L.N. Brewer, Particle deformation and microstructure evolution during cold spray of individual Al-Cu alloy powder particles, Acta Mater. 168 (2019) 13–23, http://dx.doi.org/10.1016/j.actamat.2019.01.054.

[13] D. MacDonald, S. Rahmati, B. Jodoin, W. Birtch, An economical approach to cold spray using in-line nitrogen–helium blending, J. Therm. Spray Technol. 28 (2018) http://dx.doi.org/10.1007/s11666-018-0813-0.

[14] Y. Zou, W. Qin, E. Irissou, J. Legoux, J. Szpunar, S. Yue, Effect of gas temperature on the microstructure and properties of cold sprayed copper coatings, in: Materials Science and Technology Conference and Exhibition 2009, MS and T'09, vol. 4, 2009.

[15] A. Ralls, A. Kasar, M. Daroonparvar, A. Siddaiah, P. Kumar, C. Kay, M. Misra, P. Menezes, Effect of gas propellant temperature on the microstructure, friction, and wear resistance of high-pressure cold sprayed Zr702 coatings on al6061 alloy, Coatings 12 (2022) 263, http://dx.doi.org/10.3390/coatings12020263.

[16] H. Lee, H. Shin, S. Lee, K. Ko, Effect of gas pressure on Al coatings by cold gas dynamic spray, Mater. Lett. 62 (10) (2008) 1579–1581, http://dx.doi.org/10.1016/j.matlet.2007.09.026.

[17] M. Winnicki, T. Piwowarczyk, A. Małachowska, A. Ambroziak, Effect of gas pressure and temperature on stereometric properties of al+al2o3 composite coatings deposited by LPCS method, Archives Metallurgy Mater. 59 (2014) http://dx.doi.org/10.2478/amm-2014-0149.

[18] H. Zhang, J. Zhang, A. Shan, J. Wu, H. Song, Effects of gas temperature on bonding and deformation behavior of cold-sprayed Ni particles, Acta Metallur. Sinica -Chinese Edition 43 (2007) 823–828.

[19] L. Alonso, M. Garrido-Maneiro, P. Poza, An optimisation method for the cold-spray process: On the nozzle geometry, Mater. Des. (2022) http://dx.doi.org/10.1016/j.matdes.2022.110387.

[20] B. Jodoin, Cold spray nozzle match number limitation, J. Therm. Spray Technol. 11 (2001) 496–507, http://dx.doi.org/10.1361/105996302770348628.

[21] H. Jami, A. Jabbarzadeh, Effect of particle shape on mechanics of impact in the deposition of titanium nanoparticles on a titanium substrate, Surf. Coat. Technol. 394 (2020) 125880, http://dx.doi.org/10.1016/j.surfcoat.2020.125880.

[22] I. Dowding, M. Hassani, Y. Sun, D. Veysset, K.A. Nelson, C.A. Schuh, Particle size effects in metallic microparticle impact-bonding, Acta Mater. 194 (2020) 40–48, http://dx.doi.org/10.1016/j.actamat.2020.04.044.

[23] H. Katanoda, M. Fukuhara, N. Iino, Numerical study of combination parameters for particle impact velocity and temperature in cold spray, J. Therm. Spray Technol. 16 (2007) 627–633, http://dx.doi.org/10.1007/s11666-007-9087-7.

[24] A. Moridi, S.M. Hassani-Gangaraj, M. Guagliano, M. Dao, Cold spray coating: review of material systems and future perspectives, Surface Eng. 30 (6) (2014) 369–395, http://dx.doi.org/10.1179/1743294414Y.0000000270.

[25] V. Champagne Jr., D. Helfritch, M. Trexler, B. Gabriel, The effect of cold spray impact velocity on deposit hardness, Modelling Simul. Mater. Sci. Eng. 18 (2010) 065011, http://dx.doi.org/10.1088/0965-0393/18/6/065011.

[26] W.-Y. Li, H. Liao, G. Douchy, C. Coddet, Optimal design of a cold spray nozzle by numerical analysis of particle velocity and experimental validation with 316l stainless steel powder, Mater. Des. 28 (2007) 2129–2137, http://dx.doi.org/10.1016/j.matdes.2006.05.016.

[27] R. Lupoi, Current design and performance of cold spray nozzles: experimental and numerical observations on deposition efficiency and particle velocity, Surface Eng. 30 (5) (2014) 316–322, http://dx.doi.org/10.1179/1743294413Y.0000000214.

[28] V. Champagne, D. Helfritch, S. Dinavahi, P. Leyman, Theoretical and experimental particle velocity in cold spray, J. Therm. Spray Technol. 20 (3) (2011) 425–431, http://dx.doi.org/10.1007/s11666-010-9530-z.

[29] Li, C.J and Li, W.Y and Liao, H..

[30] W.-Y. Li, C.-J. Li, H.-T. Wang, C.-X. Li, H.-S. Bang, Measurement and numerical simulation of particle velocity in cold spraying, J. Therm. Spray Technol. 15 (2006) 559–562, http://dx.doi.org/10.1361/105996306X146956.

[31] C.-J. Li, T. Wu, C.-X. Li, B. Sun, Effect of spray particle trajectory on the measurement signal of particle parameters based on thermal radiation, J. Therm. Spray Technol. 12 (2003) 80–94, http://dx.doi.org/10.1361/105996303770348537.

[32] H. Jung, J. Park, S. Park, H. Kim, C. Lee, J. Han, Effect of the expansion ratio and length ratio on a gas-particle flow in a converging-diverging cold spray nozzle, Met. Mater. Int. 15 (6) (2009) 967–970, http://dx.doi.org/10.1007/s12540-009-0967-x.

[33] T. Schmidt, F. Gärtner, H. Assadi, H. Kreye, Development of a generalized parameter window for cold spray deposition, Acta Mater. 54 (3) (2006) 729–742, http://dx.doi.org/10.1016/j.actamat.2005.10.005.